available at www.sciencedirect.com
journal homepage: www.eu-openscience.europeanurology.com

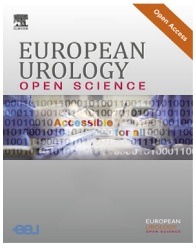

European Association of Urology

Trial Protocol

Clinical Trial Protocol: Developing an Image Classification Algorithm for Prostate Cancer Diagnosis on Three-dimensional Multiparametric Transrectal Ultrasound

Auke Jager [a,*], *Arnoud W. Postema* [a], *Massimo Mischi* [b], *Hessel Wijkstra* [b], *Harrie P. Beerlage* [a], *Jorg R. Oddens* [a]

[a] *Amsterdam UMC location University of Amsterdam, Urology, Amsterdam, The Netherlands;* [b] *Eindhoven University of Technology, Eindhoven, The Netherlands*

Article info

Article history:
Accepted December 22, 2022

Associate Editor:
Guillaume Ploussard

Keywords:
Prostate cancer
Multiparametric ultrasound
Contrast-enhanced ultrasound
Elastography
Machine learning

Abstract

Introduction and hypothesis: The tendency toward population-based screening programs for prostate cancer (PCa) is expected to increase demand for prebiopsy imaging. This study hypothesizes that a machine learning image classification algorithm for three-dimensional multiparametric transrectal prostate ultrasound (3D mpUS) can detect PCa accurately.
Design: This is a phase 2 prospective multicenter diagnostic accuracy study. A total of 715 patients will be included in a period of approximately 2 yr. Patients are eligible in case of suspected PCa for which prostate biopsy is indicated or in case of biopsy-proven PCa for which radical prostatectomy (RP) will be performed. Exclusion criteria are prior treatment for PCa or contraindications for ultrasound contrast agents (UCAs).
Protocol overview: Study participants will undergo 3D mpUS, consisting of 3D grayscale, 4D contrast-enhanced ultrasound, and 3D shear wave elastography (SWE). Whole-mount RP histopathology will provide the ground truth to train the image classification algorithm. Patients included prior to prostate biopsy will be used for subsequent preliminary validation. There is a small, anticipated risk for participants associated with the administration of a UCA. Informed consent has to be given prior to study participation, and (serious) adverse events will be reported.
Statistical analysis: The primary outcome will be the diagnostic performance of the algorithm for detecting clinically significant PCa (csPCa) on a per-voxel and a per-microregion level. Diagnostic performance will be reported as the area under the receiver operating characteristic curve. Clinically significant PCa is defined as the International Society of Urological grade group $\geq$2. Full-mount RP histopathology will be used as the reference standard. Secondary outcomes will be sensitivity, specificity, negative predictive value, and positive predictive value for csPCa on a per-patient level, evaluated in patients included prior to prostate biopsy, using biopsy results as the reference standard. A further analysis will be performed on

* Corresponding author. Amsteerdam UMC location University of Amsterdam, Urology, Meibergdreef 9, 1105 AZ, Amsterdam, The Netherlands. Tel.: +31629474347.
E-mail address: a.jager1@amsterdamumc.nl (A. Jager).

https://doi.org/10.1016/j.euros.2022.12.018

the ability of the algorithm to differentiate between low-, intermediate-, and high-risk tumors.

Discussion and summary: This study aims to develop an ultrasound-based imaging modality for PCa detection. Subsequent head-to-head validation trials with magnetic resonance imaging have to be performed in order to determine its role in clinical practice for risk stratification in patients suspected for PCa.

1. Introduction and hypothesis

Early detection of prostate cancer (PCa) is a field subject to rapid changes. The introduction of magnetic resonance imaging (MRI) has had a major impact on the diagnostic pathway for PCa.

Performing prebiopsy MRI leads to better patient selection for biopsy and improved detection of clinically significant PCa (csPCa) [1–4]. Therefore, current European guidelines strongly recommend performing MRI before biopsy [5]. The introduction of MRI has also reignited interest in population-based screening. The main argument against screening—overdiagnosis and overtreatment of insignificant PCa—has become less relevant due to improved patient selection based on risk-adapted strategies that integrate MRI [6,7]. However, the widespread integration of MRI in early detection also poses challenges concerning availability and quality [8]. First, although MRI has improved patient selection for prostate biopsy, the positive predictive value (PPV) of MRI remains limited, resulting in a substantial number of patients undergoing unnecessary biopsies [1–4,9–11]. Furthermore, in studies reporting high sensitivity, such as the 4M and PRECISION trials, MRI findings are assessed by multiple experienced uroradiologists from high-volume centers [2–4,9]. The large variability in negative predictive values (NPVs) between studies suggests that the results of these studies cannot be generalized to common clinical practice [12]. Finally, MRI is a time-consuming and costly imaging modality. Prebiopsy MRI is becoming the standard of care in more and more institutions. The resulting increase in the number of MRI scans being performed puts a strain on the already limited availability of scanning time and specialized radiologists. The current move toward population-based screening will only exacerbate this issue, resulting in longer waiting lists and a decrease in the quality of prostate MRI. Possible solutions lie in better upfront patient selection using risk-stratification tools or optimization of the radiological workflow for MRI acquisition and evaluation [8].

Another possible solution is the use of transrectal ultrasound (US) as an alternative to MRI or as a tool for better selecting patients who need MRI. US is a cost-effective and widely available imaging modality. Although conventional grayscale US has poor diagnostic accuracy for csPCa, the introduction of novel US modalities combined with computer-aided diagnosis has shown promising results [13–18]. Employing a multiparametric approach using different US modalities, such as shear wave elastography (SWE) and contrast-enhanced ultrasound (CEUS), with the extraction of quantitative features by contrast ultrasound dispersion imaging (CUDI), has resulted in a further increase in diagnostic accuracy [13,15,16,18–20].

The application of CEUS and CUDI in PCa detection is based on angiogenesis. Angiogenesis is necessary for the growth and progression of PCa and brings abnormalities in the microvascular structures [21]. These abnormalities in the microvasculature cause alternations in dispersion and perfusion of the intravenous ultrasound contrast agent (UCA), which can be visualized and quantified by CUDI. In CEUS, emitted sound waves cause oscillation of the gas-filled microbubbles within the intravenously injected UCA. This oscillation results in a characteristic nonlinear scattering of sound waves that can be visualized by contrast-specific US imaging protocols [22]. After image acquisition, CUDI quantifies the abnormalities in contrast dispersion, based on a spatiotemporal analysis of the time intensity curves (TICs) extracted for each pixel on the CEUS image. These TICs show location-specific contrast intensity evolution over time [23–26]. The parametric maps resulting from CUDI can be used to visualize areas suspected for PCa.

SWE is developed to visualize and quantify stiff lesions in soft tissue [27]. SWE uses US radiation force to generate shear waves and measures their propagation speed through the target tissue. Absolute prostate tissue stiffness can then be quantified by converting the shear wave speed into the Young's modulus (expressed in kilopascal). The Young's modulus can be visualized in real time on a color-coded map that is overlaid on regular grayscale imaging [27–30].

Multiple studies have shown the potential of these novel US modalities. When comparing CEUS and CUDI parametric analysis with full gland histopathology, sensitivity up to 83% was shown for csPCa localization, which is similar to studies correlating MRI with whole-mount prostate pathology [19,31–34]. Studies comparing SWE with full gland histopathology show an evident relation between stiffness of tissue (measured using the Young's modulus) and the presence of PCa [35,36]. A recent systematic review on the diagnostic accuracy of SWE, including 16 studies with a total of 2277 patients, found varying results with pooled sensitivities and specificities for PCa detection ranging from 0.71 to 0.87 and from 0.69 to 0.85, respectively [30]. The same studies show the stiffness of PCa lesions to increase with higher Gleason scores (GSs), with the median Young's modulus values of 42, 37, and 68 kPa for GSs 5–6, 7, and 8–9, respectively [36]. When combing the different US modalities in a multiparametric approach, the diagnostic accuracy

increases. A study evaluating quantitative parameters and radiomic features extracted from the brightness mode (B-mode), CEUS, and SWE found an area under the receiver operating characteristic (AUROC) curve of 0.90 for csPCa [13]. In this study, the multiparametric approach showed a clear benefit, with the best performing single parameter reaching an AUROC of 0.84 [13]. Finally, a head-to-head trial comparing targeted biopsies based on CUDI and MRI found comparable results for both modalities, with csPCa detection of 28% and 29%, respectively [37].

A major limitation of studies evaluating transrectal multiparametric ultrasound (mpUS) for PCa diagnosis resides in the two-dimensional (2D) image acquisition. In 2D CEUS, each plane needs to be imaged separately. Imaging a single plane takes 2 min plus a 3-min UCA washout period, and each plane requires the administration of a new bolus of the UCA, making it a time-consuming procedure. Recent advances in US technology have made dynamic 3D acquisitions possible, thereby facilitating visualization of the whole prostate enhancement for 2 min, using one single bolus of the UCA. Following these advances, Wildeboer et al [14,38] evaluated 3D CEUS and CUDI parameters for csPCa detection. They showed the feasibility of the multiparametric approach in a 3D setting, reaching an AUROC of 0.81 by applying machine learning (ML) on a dataset of 3D US images from 43 patients undergoing prostate biopsies [14].

A computer-aided and multiparametric approach to transrectal US of the prostate has shown potential for the detection of csPCa. By correlating 3D mpUS images with a reliable ground truth, an artificial intelligence (AI)-based image classification algorithm can be created and validated as a diagnostic tool for the detection of PCa. If the diagnostic performance of the algorithm is sufficient, it will be a valuable triage tool in early detection programs for PCa.

2. Design

This study is a phase 2 multicenter diagnostic accuracy trial conducted in The Netherlands.

2.1. Study population

The study consists of two cohorts of patients: (1) patients with a clinical suspicion for PCa planned for prostate biopsy and (2) patients with biopsy-proven PCa planned for radical prostatectomy (RP). A total of 715 patients will be included in this trial over an expected period of 2 yr. The inclusion and exclusion criteria are provided in Table 1.

3. Protocol overview

A flowchart of the study design for both study groups is provided in Figure 1.

Clinical patient data concerning demographics, cancer-specific characteristics, pathology, and radiology reports are collected in a Castor EDC database. An overview of all patient data collected in the database is provided in the Supplementary material.

Table 1 – Inclusion and exclusion criteria

Inclusion criteria:
1. Men ≥18 yr
2. Clinical suspicion of prostate cancer or biopsy-proven prostate cancer
3. Scheduled for either systematic and/or targeted biopsy or radical prostatectomy
4. MRI performed within 1 yr prior to prostate biopsy or radical prostatectomy
Exclusion criteria:
1. Prostate biopsy within the past 30 d
2. Chemotherapy, radiation therapy, and/or focal treatment for prostate cancer
3. Hormonal treatment for prostate cancer within the past 6 mo
4. Any of the following contraindications for the intravenous ultrasound contrast agent: cardiac right to left shunt, pulmonary hypertension, uncontrolled systemic hypertension, respiratory distress syndrome, previous allergic reaction, and current treatment with dopamine

MRI = magnetic resonance imaging.

4. Study procedure

4.1. Three-dimensional mpUS

Three-dimensional mpUS will be performed using the GE LOGIQ E10 US machine with a RIC 5-9D transrectal probe and will consist of consecutively 3D B-mode, 3D SWE, and 4D CEUS. The study protocol defines standardized settings (eg, frequency, gain, dynamic range, and mechanical index) for each US acquisition. Intravenous access will be secured for UCA administration. US will be performed with the patient in the lithotomy position. The total imaging time is expected to be approximately 8 min. All 3D mpUS imaging procedures will be performed by an operator with experience in transrectal US imaging, after receiving training on the different US modalities used in this trial.

4.2. Three-dimensional B-mode imaging

Prior to grayscale acquisition, the transrectal probe has to be positioned properly, ensuring that the entire prostate is visualized and centered in the transversal and sagittal plane. The US depth and window can be adjusted when necessary. The probe is secured in place using a custom made probe fixture (see Fig. 2) to ensure stable image acquisition during the entire study procedure. The 3D acquisition option on the US machines allows rapid B-mode imaging (approximately 1 s) of the entire prostate.

4.3. Three-dimensional SWE

Using a macro feature programmed on the US machine, the 3D SWE mode is performed. This macro captures 25 SWE images every 5° over a 120° angle from the basal to the apical side of the prostate.

4.4. Four-dimensional CEUS

Prior to 4D CEUS acquisition, a single bolus (2.4 ml) of UCA (SonoVue; Bracco, Geneva, Switzerland) followed by a 10-ml NaCl 0.9% flush is administered intravenously. Directly after UCA administration, a 2-min 4D CEUS recording is performed. The machine allows for a volume rate of approximately 1 s, meaning that one 3D CEUS image is acquired every second.

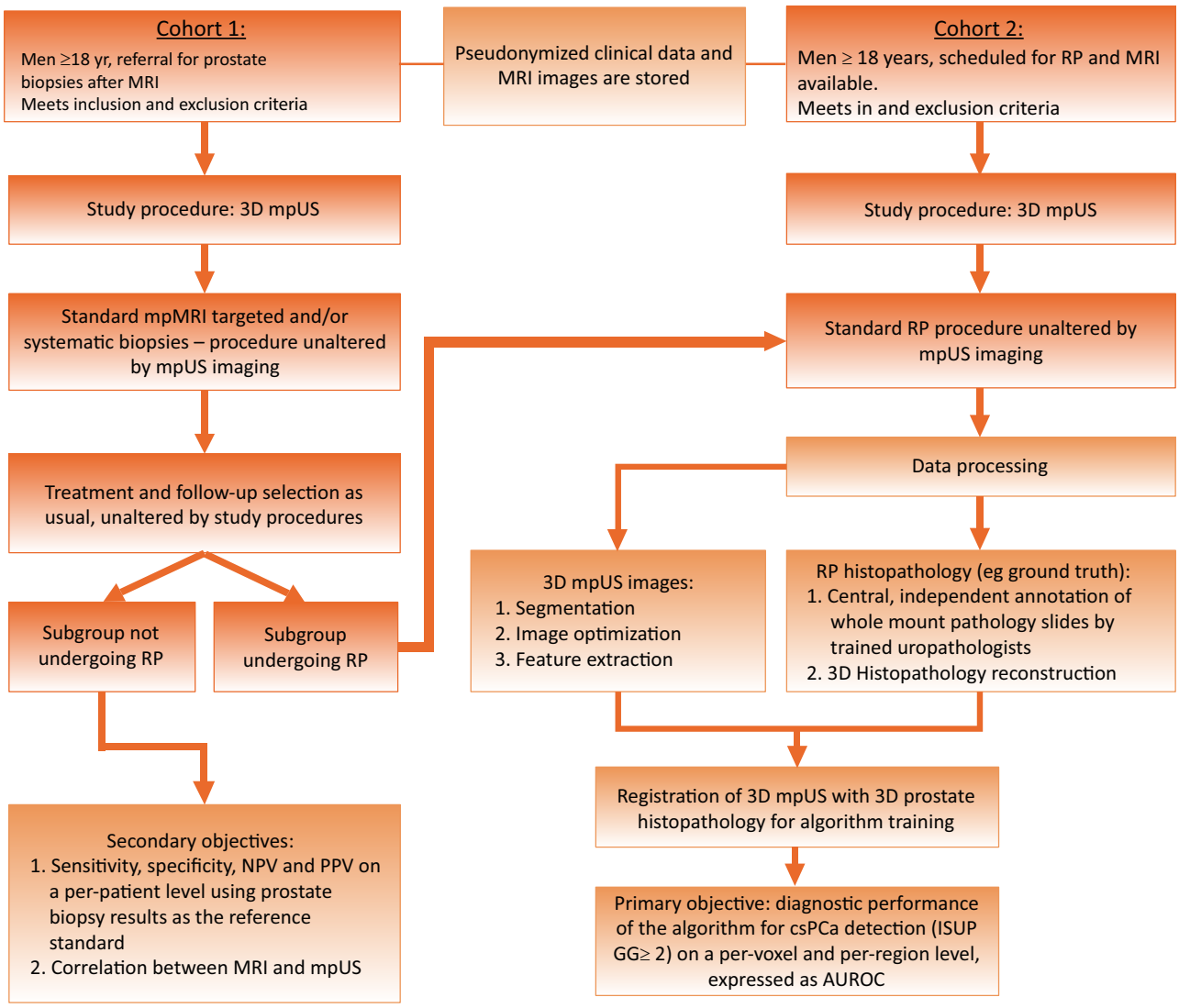

Fig. 1 – Study flowchart. AUROC = area under the receiver operating characteristic; csPCa = clinically significant prostate cancer; 3D = three dimensional; ISUP GG = International Society of Urological Pathology grade group; mpUS = multiparametric ultrasound; MRI = magnetic resonance imaging; NPV = negative predictive value; PPV = positive predictive value; RP = radical prostatectomy.

5. Data processing

The quality of the algorithm depends on the quality of the input (ie, the ground truth). In the current study, 3D whole-mount prostate histopathology will be used as the ground truth. Accurate registration of pathology with US is challenging due to tissue deformation both during imaging and after surgery. To provide a reliable ground truth, the current study has devised a step-wise protocol for data processing: (1) US image segmentation, (2) whole-mount RP histopathology annotation and 3D reconstruction, and (3) registration of 3D US with 3D prostate histopathology.

1. US image segmentation: US images are segmented by two clinicians with >2 yr of experience with performing prostate US and biopsy. Segmentations are performed using software custom designed for this study. For all scans, the prostate border, peripheral zone (PZ), and urethra are segmented. Visible ejaculatory ducts are segmented as well. Other structures visible on both pathology and US images ("landmarks"), such as calcifications or prostatic utricle cysts, can be annotated to further increase registration accuracy. Figure 3 shows an illustration of the US image segmentation process and the resulting 3D US model.

2. Whole-mount RP histopathology annotation and 3D reconstruction: RPs will be performed in high-volume centers according to the local protocol. Prostate specimens will be treated according to the study protocol. The study protocol will not affect histopathological evaluation for clinical purposes. Prior to fixation in formalin, four intravenous cannulas will be inserted from the apex to the base in four quadrants. The resulting needle holes are used to accurately stack slices for 3D pathology reconstruction (Fig. 4). After fixation in formalin, the prostate is divided into 4-mm thick slices, in the transversal plane, from the apex to the base, using the TruSlice specimen cut-up system (CellPath Ltd, Newtown, UK). A high-resolution macrophoto is taken of the prostate slices, including a scale for reference. Whole-mount slices will be fitted into cassettes, embedded in paraffin, and cut into pathology slides using a microtome. Whole-mount pathology slides are scanned on high

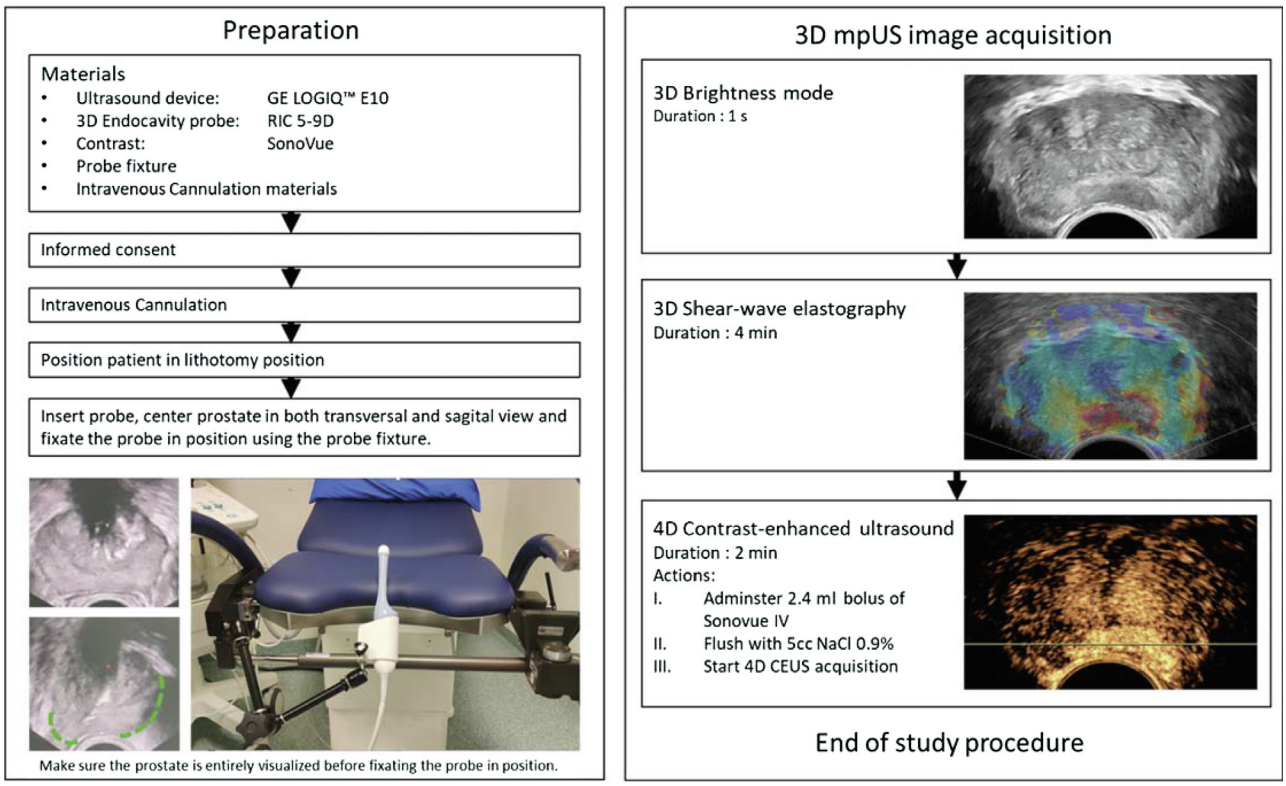

Fig. 2 – Study procedure. CEUS = contrast-enhanced ultrasound; 3D = three dimensional; 4D = four dimensional; IV = intravenous; mpUS = multiparametric ultrasound.

resolution (40× enlargement, 20× objective, 2.1 camera lens) using a Pannoramic 1000 Digital Slide Scanner (3DHISTECH, Budapest, Hungary) and uploaded to a web-based pathology annotation tool (Slidescore; Slide Score B.V., Amsterdam, The Netherlands). Digitized slides will be annotated by dedicated genitourinary pathologists, blinded for clinical data. The study protocol dictates precise delineation of the following tissue types (if present): Gleason patterns 3–5; Gleason pattern 4 with cribriform growth (CG) and/or intraductal carcinoma (IDC), high-grade prostatic intraepithelial neoplasia (HG-PIN), and prostatitis. For registration purposes, the prostate border, PZ, urethra, and (if visible) landmarks will be annotated as well. The full version of the standard operating procedure of the annotation protocol is provided in the Supplementary material. Figure 5 shows an example of a pathology slide annotated according to the study protocol. After pathology annotation, the pathology slides are overlaid on the macroscopic prostate slices and stacked to create a 3D histopathology model (Fig. 4).

3. Registration of US and pathology: The final step in creating the ground truth is the registration of the 3D prostate pathology model onto the corresponding 3D US. Image registration methods used in this trial expand on previously described methods [18,39]. Two surface meshes from the outer contours of the prostate are constructed, one based on delineation of the prostate borders on US and one on the prostate borders of the pathology slides. Rigid and elastic registration methods are used to compensate for deformation and shrinking of the prostate specimen and for deformation of the prostate during imaging due to the pressure of the probe. Anatomical landmarks such as the urethra, border of PZ and transitional zone (TZ), and ejaculatory ducts are used to increase and evaluate the accuracy registration. Figure 6 shows the steps of the current registration protocol.

5.1. *Image processing and feature extraction*

To improve the quality of the data, preprocessing is performed for resolution equalization, noise suppression, motion, and deformation compensation [40]. Prostate zonal segmentation is performed manually (Fig. 3) to allow for voxel labeling (ie, belonging to PZ or not). Zonal labeling is considered important for several reasons: tissue characteristics of the PZ and TZ lead to differences in tissue stiffness and UCA flow, causing substantial differences in the selected features [13,39,41]. Additionally, it is well established that the PZ and TZ provide distinct probabilities for the presence of PCa [42,43].

Subsequent feature extraction will entail execution of modules that compute perfusion and dispersion parameters (by both temporal and spatiotemporal analysis of the extracted TICs), as well as other characteristics of the microvascular network by the fractal dimension, mutual information, and entropy of velocity fields [14,17,23–26,38,44]. Young's modulus will be derived from SWE as a measure for tissue elasticity. Grayscale imaging will be used for zonal segmentation and calcification analysis.

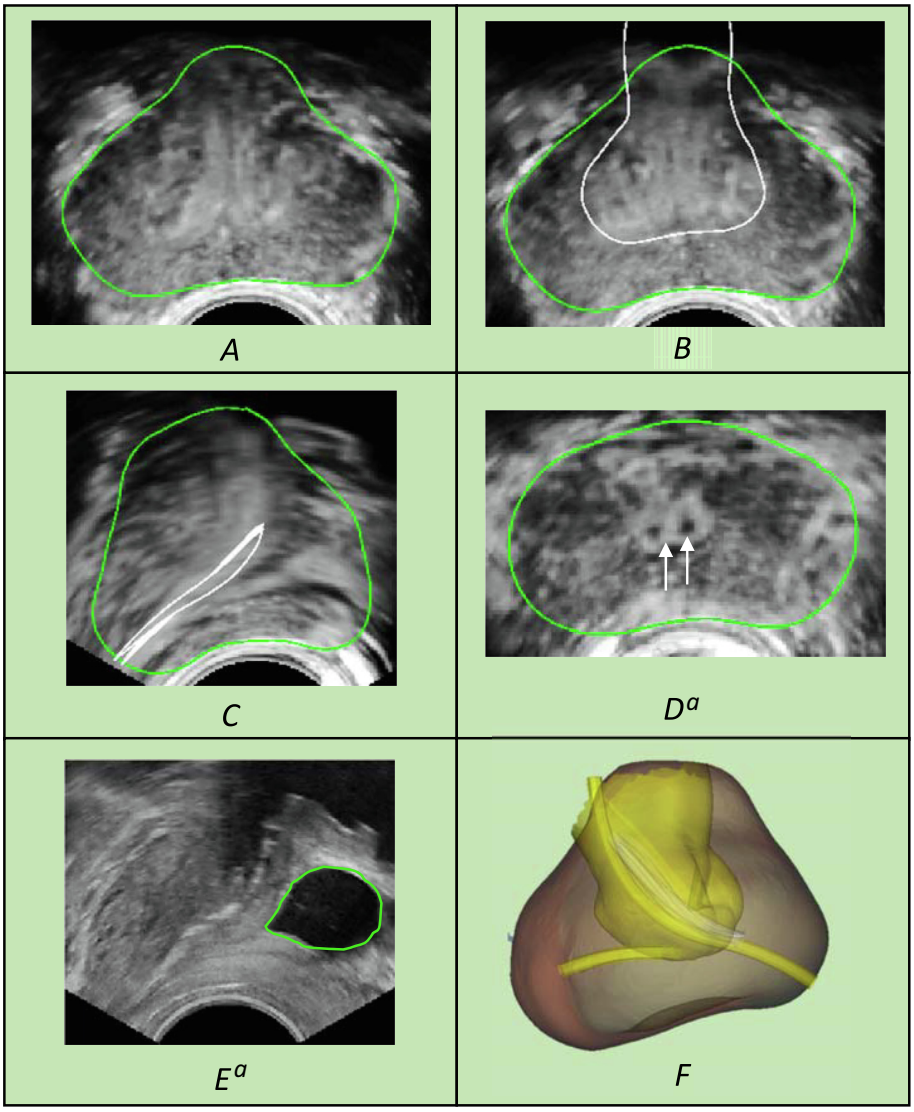

Fig. 3 – Ultrasound image segmentation. Images from a contrast-enhanced ultrasound from a single patient: (A) prostate border, (B) border between PZ and TZ, (C) urethra, and (D) ejaculatory ducts. (E) A brightness-mode ultrasound image from a different patient: example of a landmark (prostatic utricle cyst). (F) A 3D model of the prostate based on segmentation shown in (A–D). 3D = three dimensional; PZ = peripheral zone; TZ = transitional zone. [a] Ejaculatory ducts and landmarks can be used for more accurate registration, but are not visible for all patients.

5.2. Training and validation of the ML algorithm

As a result, each of the resulting features provides a relevant characteristic of a voxel in one of the coregistered scans within the context of a local region of interest. This leaves us with a set of 3D spatially discrete scalar fields, one for each feature.

An ML classification algorithm will be used to combine these features into a local prediction for the presence of csPCa. Such local prediction is performed either on a per-voxel basis or for a cube of voxels, which we refer to as a micro region.

For voxel-based classification, we will consider the following ML classification algorithms: linear support vector machines (SVMs) and gradient boosting, using XGBoost as well as a 3D convolutional neural network. Each of these techniques will classify individual voxels and will also provide a confidence metric. By combining these, it will be possible to counter some of the prediction errors in individual voxels and provide a coherent spatial prediction, matching known spatial correlation properties in lesion shapes, as derived from the histology annotations.

A second approach is to use the estimates of statistical properties, such as percentiles and statistical moments of features within a micro region. These features can be used directly by classification algorithms such as SVM and XGBoost. Owing to the very significant set of features this yields, a careful feature selection procedure will be needed.

Both voxel- and region-based predictions can be used to assess performance at patient level, where each patient for whom the classifier identifies a minimum positive predicted volume (eg, one micro region or the equivalent of >0.3 cc in voxels) is designated as positive.

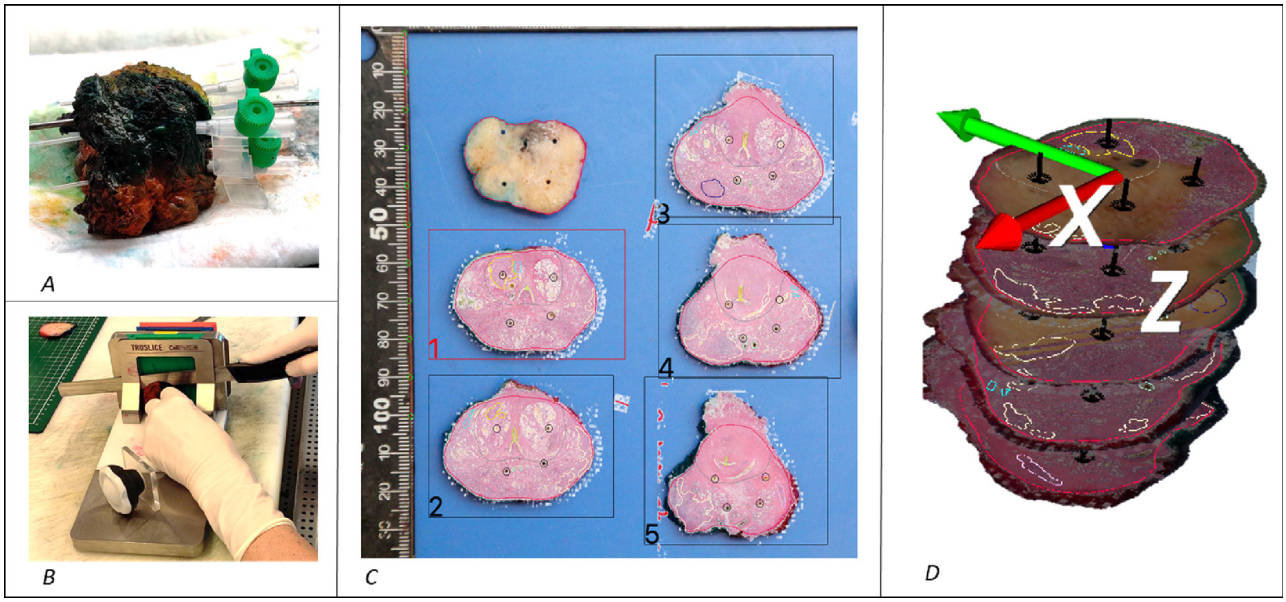

Fig. 4 – Prostate pathology reconstruction. (A) Intravenous cannulas are inserted from the apex to the base prior to prostate specimen fixation. (B) After fixation, the prostate is divided into 4-mm thick slices. (C) Annotated whole-mount pathology slides are overlaid on the macroscopic prostate slices. (D) Pathology slides are stacked to create a 3D prostate pathology model; needle holes are used to prevent rotational and transitional errors. 3D = three dimensional.

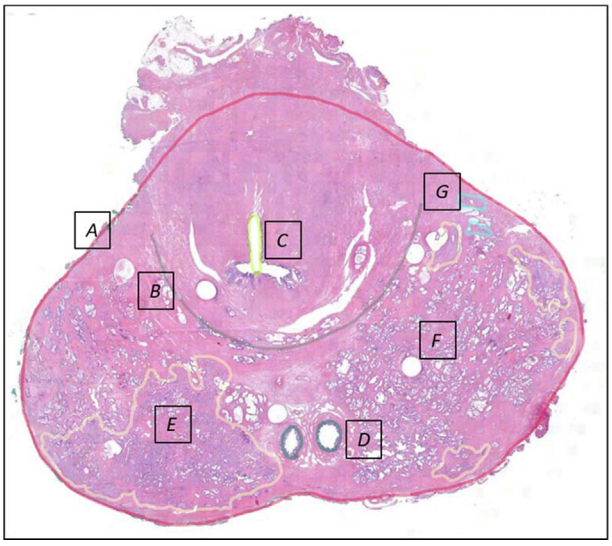

Fig. 5 – Full-mount prostate pathology slide annotated according to the study protocol. Slide originates from the same prostate shown in Figures 3A–D and 3F: (A) prostate border, (B) border between PZ and TZ, (C) urethra, (D) ejaculatory ducts, (E) Gleason score 3 + 4 = 7 PCa, (F) needle hole from cannulas inserted prior to slicing the prostate specimen, and (G) Gleason Pattern 3. PCa = prostate cancer; PZ = peripheral zone; TZ = transitional zone.

The use of relatively small data sets such as these bares the risk of overestimating generalization performance. Therefore, we will use a nested cross-validation (CV) approach when optimizing any of the hyper parameters, feature selections, and model comparison. The used CV folds will be based on groups, grouping voxels on a per-patient basis, such that data from one patient will never be used in both training and test or validation set.

6. Statistical analysis

6.1. *Primary outcome*

The diagnostic performance of the ML-based image classification algorithm for csPCa diagnosis on 3D mpUS will be reported as an AUROC, with 95% confidence intervals, on a per-voxel ($0.75 \times 0.75 \times 0.75$ mm^3) and a per-microregion (2 cm^3) level using whole-mount prostate histopathology as the ground truth and reference standard. Clinically significant PCa will be defined as International Society of Urological Pathology (ISUP) grade group (GG) $\geq$2. A lesion will be defined as ISUP GG $\geq$2 with a volume of $\geq$0.3 ml.

6.2. *Secondary outcomes*

Multiple additional outcomes will be evaluated for each study arm.

Study cohort 1 (biopsy cohort):

1. Sensitivity, specificity, PPV, and NPV of 3D mpUS for the presence of csPCa at prostate biopsy on a per-patient level.

Study cohort 2 (pre-RP cohort):

1. Sensitivity for the detection of the index lesion. The index lesion is defined as the lesion with the highest ISUP GG, or, in case of multiple lesions with the same ISUP GG, the lesion with the highest volume. A further analysis will be carried out on correct characterization of the index lesion (eg, ISUP GG, CG, and/or IDC).
2. False-positive and -negative 3D mpUS results will be analyzed on possible explanations (eg, prostatitis, HG-PIN, and calcifications).

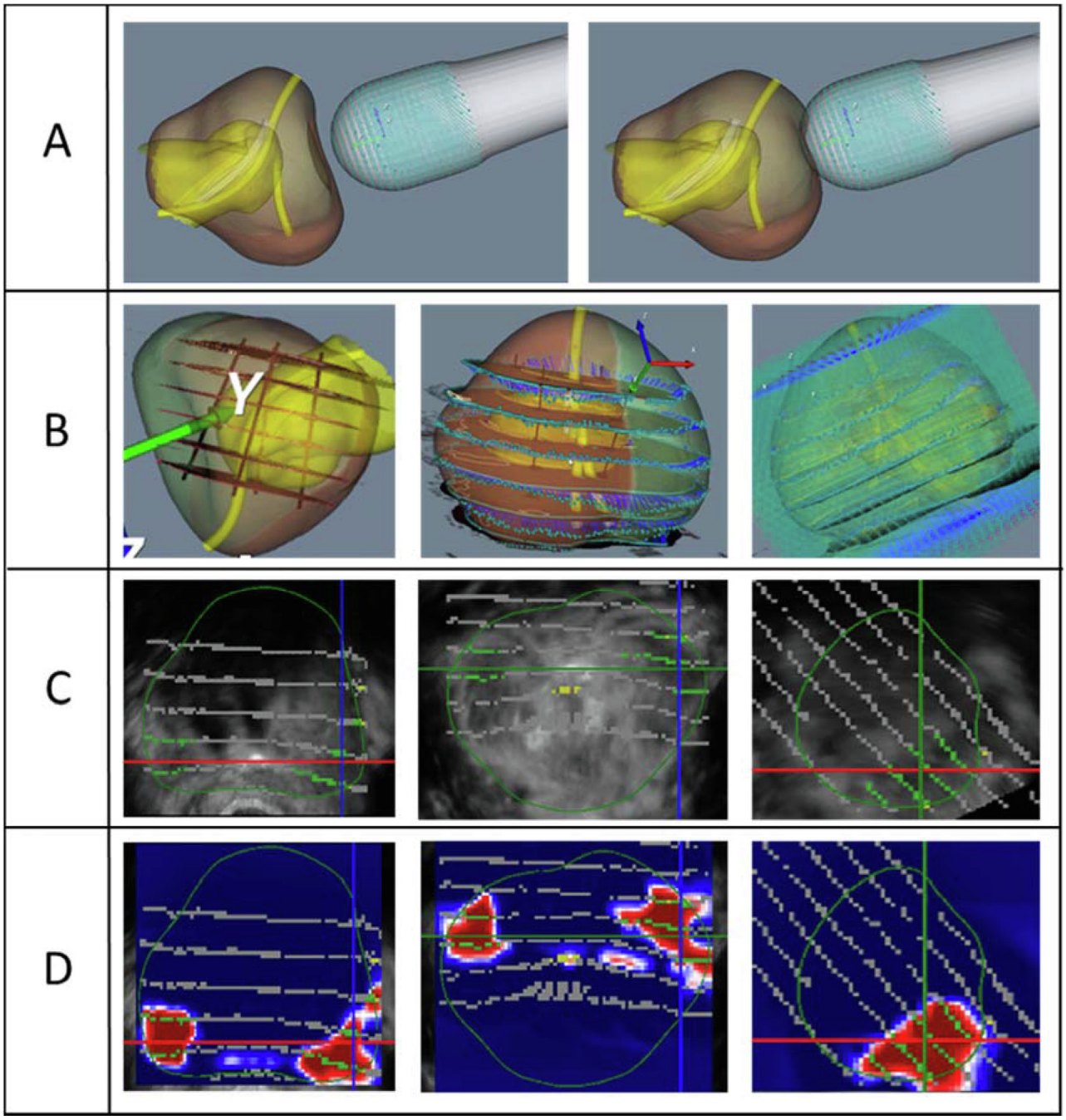

Fig. 6 – Final steps in the registration protocol: (A) Compensation for the deformation induced by the pressure of the transrectal probe on the prostate. (B) From left to right: fitting of the 3D pathology model in the 3D mpUS model, rigid registration, and elastic registration. (C) Fitted pathology sliced on the original mpUS images. In gray, the pathology slices are visualized; the green areas are the areas marked by the pathologist as containing csPCa. (D) The ground truth. The red areas are the areas marked by the pathologist as containing csPCa. The areas as visualized are an overlay on the original mpUS images. csPCa = clinically significant prostate cancer; 3D = three dimensional; mpUS = multiparametric ultrasound.

7. Sample size calculation

To train an AI-based algorithm to differentiate between certain categories (eg, benign vs insignificant PCa vs csPCa), high-quality data with a sufficient number of findings across the various outcome categories are required. The key differentiation relevant for clinical practice is the ISUP GG, based on histopathological differentiation, ranging from 1 (well-differentiated, indolent PCa) to 5 (only poorly formed glands and necrosis, high-risk disease) [45]. Based on previous experience, we expect that a minimum of 20 patients in each GG will provide an adequate amount of data for algorithm training [13]. The sample size calculation is therefore designed to ensure a sufficient number of the least frequently occurring GGs (4 and 5). The expected distribution of GGs among men undergoing RP, based on a local cohort from 2013 to 2015, is as follows: 33% are diagnosed with GG1, 38% diagnosed with GG2, 15% diagnosed with GG3, 7% diagnosed with GG4, and 7% diagnosed with

GG5 [18]. To obtain a minimum of 20 patients in GG4 and GG5, the target sample size for RP specimens is therefore 286 (20 × 100/7). It is noted that due to the shift toward active surveillance in men with GG1, it is likely that the current GG distribution will also have shifted toward higher GGs; therefore, an interim analysis will be done when 66% (181) of the target sample size for RP patients is reached.

In order to reduce sample bias and perform a preliminary assessment of 3D mpUS in a representative target population, patients with a clinical suspicion for PCa, planned for prostate biopsy, will be included in the cohort as well. Data originating from the Cochrane meta-analysis find that approximately 40% of patients undergoing prostate biopsies are diagnosed with csPCa [1]. To achieve a study population comparable with the general population, we aim to adhere to these statistics. Therefore, the 286 prostatectomy patients (patients with csPCa) who will be included in this trial represent 40% of the total cohort, with the remaining 60% representing the population with no PCa or no csPCa diagnosis. The total sample size therefore amounts to 715 (100 × 286/40).

8. Risks and benefits

There are no direct benefits for patients participating in this study. However, results originating from this trial could significantly improve the diagnostic workup for future patients with a clinical suspicion for PCa. The burden and risk associated with participation in this study are limited. There is a small anticipated risk for participants associated with the administration of UCA. The UCA used in this study is extensively studied and approved by the European Medicines Agency for intravenous use. Adverse events caused by the UCA are generally mild and transient. The side effects of the UCA mostly consist of transient alteration of taste, local pain at the injection site, and facial or general flush. In rare cases (<0.01%), serious adverse events, consisting of allergic reactions, are described [46–48]. Patients will receive extensive information concerning the risks and absence of benefits, and informed consent has to be given prior to study participation. This study was approved by an accredited medical research ethics committee (MEC AMC).

9. Discussion

Novel US modalities, such as CUDI and SWE, are promising diagnostic imaging modalities for early detection programs for PCa, reaching similar diagnostic accuracy to the current standard: MRI [37]. More recently, the feasibility of a multiparametric ML approach for US was demonstrated. Wildeboer et al [13] combined features originating from different US modalities (CEUS, B-mode, and SWE) into classifiers through ML, reaching an AUROC of 0.90 for csPCa. The same group proved that the multiparametric approach

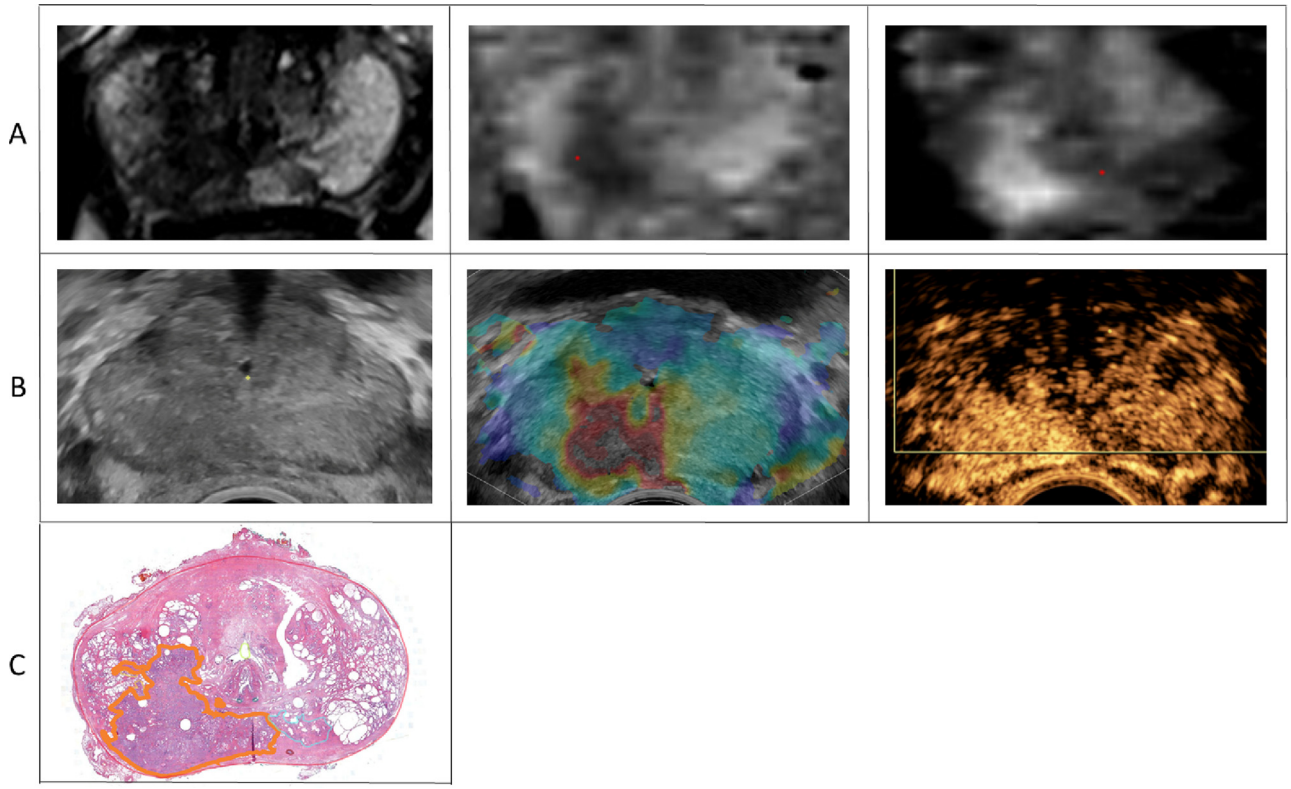

Fig. 7 – Example of a significant prostate cancer lesion visible on both MRI and mpUS. (A) Biparametric MRI sequences from left to right: T2 weighted, ADC, and DWI. PI-RADS 5 lesion in the right peripheral zone, 22 × 11 × 10 mm^3. Minimal ADC value of 634. (B) Multiparametric ultrasound images, from left to right: B-mode, SWE and CEUS. Right peripheral zone shows hypoechogenic lesion on B-mode and correlates with an area of increased tissue stiffness on SWE and early enhancement on CEUS. (C) Whole-mount pathology shows a Gleason Score of 4 + 3 = 7 with >80% Gleason pattern 4 (annotated in orange). Lesion location corresponds to both MRI and mpUS lesions. ADC = apparent diffusion coefficient; B-mode = brightness mode; CEUS = contrast-enhanced ultrasound; DWI = diffusion weighted imaging; mpUS = multiparametric ultrasound; MRI = magnetic resonance imaging; PI-RADS = Prostate Imaging Reporting and Data System; SWE = shear-wave elastography.

is translatable into 3D [14]. The potential for PCa detection of the different US-based imaging modalities is clearly illustrated in Figure 7.

Limitations of prior studies are the small sample sizes and their 2D image acquisition. The current study will expand on previous studies by providing a larger dataset, consisting of 3D images, acquired in a multicenter setting.

There are multiple aspects of the current study design that have to be taken into consideration. The quality of the algorithm is highly dependent on the quality of the ground truth. The quality of the ground truth relies on the reliability of the pathology annotations and the accuracy of registration.

To optimize the reliability of the pathology annotations, a study-specific protocol was composed in cooperation with five experienced uropathologists. An important factor that influences the quality of the data is the interobserver variability. In a clinical setting, interobserver variability in Gleason grading varies from fair to substantial [49–51]. A study is currently being conducted to analyze the per pathology slide and the surface-based interobserver variability when annotating according to the study protocol.

Registration errors can occur when matching the 3D US images with the 3D prostate histopathology model, due to prostate deformation during US imaging, surgery, and the histopathological process, and due to prostate shrinkage during fixation in formalin. The reconstruction protocol, as described in the methods section, is designed to minimize the error during registration. Anatomical landmarks, such as the urethra, the border between the PZ and TZ and ejaculatory ducts, will be used to quantify errors and evaluate the accuracy of the reconstruction and registration protocol.

The design of the current study has some limitations. First, the algorithm will be trained primarily on data originating from patients undergoing RP, which inherently comes with a selection bias. However, considering that data collection will be performed per voxel, and each patient will provide voxels with and without PCa, it is expected that the training set will contain sufficient data on malignant as well as benign voxels. Ultimately, the algorithm will have to be validated on a more representative cohort. The current study includes assessment of the diagnostic performance of 3D mpUS, but it will not provide the data necessary for clinical validation. In the study cohort that will be included prior to prostate biopsy, an analysis will be done on the predictive values of 3D mpUS with respect to biopsy outcome. However, a comparison with the current standard of care (MRI) will not be possible. In this study, mpUS will play no role in diagnostic decision-making, and diagnostic accuracy will be assessed retrospectively. Future clinical validation trials, which include a head-to-head comparison between targeted biopsies using 3D mpUS and MRI, will have to prove that 3D mpUS is noninferior to MRI for csPCa detection.

This trial aims to provide sufficient data for the development of an ML algorithm that can detect PCa on 3D mpUS imaging. If this trial is successful, it will serve as the foundation for subsequent international clinical validation trials, with the goal to develop an US-based imaging modality that can be used as a diagnostic tool in early detection of PCa.

10. Summary

This trial protocol hypothesizes that an ML-based 3D mpUS image classification algorithm will be able to detect PCa accurately. If the hypothesis proves correct, 3D mpUS could be a relatively cost-effective and easily assessable risk-stratification tool.

***Author contributions*:** Auke Jager had full access to all the data in the study and takes responsibility for the integrity of the data and the accuracy of the data analysis.

Study concept and design: Jager, Postema, Mischi, Wijkstra, Beerlage, Oddens.
Acquisition of data: Jager, Postema.
Analysis and interpretation of data: None.
Drafting of the manuscript: Jager.
Critical revision of the manuscript for important intellectual content: Jager, Postema, Mischi, Wijkstra, Beerlage, Oddens.
Statistical analysis: None.
Obtaining funding: Mischi, Wijkstra, Beerlage, Oddens.
Administrative, technical, or material support: Jager.
Supervision: Mischi, Wijkstra, Beerlage, Oddens.
Other: None.

Financial disclosures: Auke Jager certifies that all conflicts of interest, including specific financial interests and relationships and affiliations relevant to the subject matter or materials discussed in the manuscript (eg, employment/affiliation, grants or funding, consultancies, honoraria, stock ownership or options, expert testimony, royalties, or patents filed, received, or pending), are the following: Arnoud W. Postema is a scientific advisor for Angiogenesis Analytics for which he receives compensation. Massimo Mischi is a scientific advisor for Angiogenesis Analytics for which he receives compensation. Hessel Wijkstra is a scientific advisor for Angiogenesis Analytics for which he receives compensation. Harrie Beerlage is chief of the clinical board for Angiogenesis Analytics.

***Funding/Support and role of the sponsor*:** This work was supported by Angiogenesis Analytics.

References

[1] Drost FH, Osses D, Nieboer D, et al. Prostate magnetic resonance imaging, with or without magnetic resonance imaging-targeted biopsy, and systematic biopsy for detecting prostate cancer: a Cochrane systematic review and meta-analysis. Eur Urol 2020;77:78–94.
[2] van der Leest M, Cornel E, Israel B, et al. Head-to-head comparison of transrectal ultrasound-guided prostate biopsy versus multiparametric prostate resonance imaging with subsequent magnetic resonance-guided biopsy in biopsy-naive men with elevated prostate-specific antigen: a large prospective multicenter clinical study. Eur Urol 2019;75:570–8.
[3] Kasivisvanathan V, Rannikko AS, Borghi M, et al. MRI-targeted or standard biopsy for prostate-cancer diagnosis. N Engl J Med 2018;378:1767–77.
[4] Rouviere O, Puech P, Renard-Penna R, et al. Use of prostate systematic and targeted biopsy on the basis of multiparametric MRI in biopsy-naive patients (MRI-FIRST): a prospective, multicentre, paired diagnostic study. Lancet Oncol 2019;20:100–9.
[5] Mottet N, van den Bergh RCN, Briers E, et al. EAU-EANM-ESTRO-ESUR-SIOG guidelines on prostate cancer—2020 update. Part 1: screening, diagnosis, and local treatment with curative intent. Eur Urol 2021;79:243–62.

[6] Moyer VA, Force USPST. Screening for prostate cancer: U.S. Preventive Services Task Force recommendation statement. Ann Intern Med 2012;157:120–34.
[7] Van Poppel H, Roobol MJ, Chapple CR, et al. Prostate-specific antigen testing as part of a risk-adapted early detection strategy for prostate cancer: European Association of Urology position and recommendations for 2021. Eur Urol 2021;80:703–11.
[8] de Rooij M, van Poppel H, Barentsz JO. Risk stratification and artificial intelligence in early magnetic resonance imaging-based detection of prostate cancer. Eur Urol Focus 2022;8:1187–91.
[9] El-Shater Bosaily A, Parker C, et al. PROMIS–Prostate MR imaging study: a paired validating cohort study evaluating the role of multi-parametric MRI in men with clinical suspicion of prostate cancer. Contemp Clin Trials 2015;42:26–40.
[10] Kohestani K, Wallstrom J, Dehlfors N, et al. Performance and inter-observer variability of prostate MRI (PI-RADS version 2) outside high-volume centres. Scand J Urol 2019;53:304–11.
[11] Hietikko R, Kilpelainen TP, Kenttamies A, et al. Expected impact of MRI-related interreader variability on ProScreen prostate cancer screening trial: a pre-trial validation study. Cancer Imaging 2020;20:72.
[12] Sathianathen NJ, Omer A, Harriss E, et al. Negative predictive value of multiparametric magnetic resonance imaging in the detection of clinically significant prostate cancer in the Prostate Imaging Reporting and Data System era: a systematic review and meta-analysis. Eur Urol 2020;78:402–14.
[13] Wildeboer RR, Mannaerts CK, van Sloun RJG, et al. Automated multiparametric localization of prostate cancer based on B-mode, shear-wave elastography, and contrast-enhanced ultrasound radiomics. Eur Radiol 2020;30:806–15.
[14] Wildeboer RR, van Sloun RJG, Huang P, Wijkstra H, Mischi M. 3-D multi-parametric contrast-enhanced ultrasound for the prediction of prostate cancer. Ultrasound Med Biol 2019;45:2713–24.
[15] Postema A, Idzenga T, Mischi M, Frinking P, de la Rosette J, Wijkstra H. Ultrasound modalities and quantification: developments of multiparametric ultrasonography, a new modality to detect, localize and target prostatic tumors. Curr Opin Urol 2015;25:191–7.
[16] Brock M, Eggert T, Palisaar RJ, et al. Multiparametric ultrasound of the prostate: adding contrast enhanced ultrasound to real-time elastography to detect histopathologically confirmed cancer. J Urol 2013;189:93–8.
[17] Schalk SG, Huang J, Li J, et al. 3-D quantitative dynamic contrast ultrasound for prostate cancer localization. Ultrasound Med Biol 2018;44:807–14.
[18] Wildeboer RR, Postema AW, Demi L, Kuenen MPJ, Wijkstra H, Mischi M. Multiparametric dynamic contrast-enhanced ultrasound imaging of prostate cancer. Eur Radiol 2017;27:3226–34.
[19] Mannaerts CK, Wildeboer RR, Postema AW, et al. Multiparametric ultrasound: evaluation of greyscale, shear wave elastography and contrast-enhanced ultrasound for prostate cancer detection and localization in correlation to radical prostatectomy specimens. BMC Urol 2018;18:98.
[20] Postema A, Mischi M, de la Rosette J, Wijkstra H. Multiparametric ultrasound in the detection of prostate cancer: a systematic review. World J Urol 2015;33:1651–9.
[21] Russo G, Mischi M, Scheepens W, De la Rosette JJ, Wijkstra H. Angiogenesis in prostate cancer: onset, progression and imaging. BJU Int 2012;110(11 Pt C):E794–808.
[22] Turco S, Frinking P, Wildeboer R, et al. Contrast-enhanced ultrasound quantification: from kinetic modeling to machine learning. Ultrasound Med Biol 2020;46:518–43.
[23] Kuenen MP, Saidov TA, Wijkstra H, Mischi M. Contrast-ultrasound dispersion imaging for prostate cancer localization by improved spatiotemporal similarity analysis. Ultrasound Med Biol 2013;39:1631–41.
[24] Kuenen MP, Mischi M, Wijkstra H. Contrast-ultrasound diffusion imaging for localization of prostate cancer. IEEE Trans Med Imaging 2011;30:1493–502.
[25] Mischi M, Kuenen MP, Wijkstra H. Angiogenesis imaging by spatiotemporal analysis of ultrasound contrast agent dispersion kinetics. IEEE Trans Ultrason Ferroelectr Freq Control 2012;59:621–9.
[26] van Sloun RJG, Demi L, Postema AW, De La Rosette JJMCH, Wijkstra H, Mischi M. Entropy of ultrasound-contrast-agent velocity fields for angiogenesis imaging in prostate cancer. IEEE Trans Med Imaging 2017;36:826–37.
[27] Bercoff J, Chaffai S, Tanter M, et al. In vivo breast tumor detection using transient elastography. Ultrasound Med Biol 2003;29:1387–96.
[28] Correas JM, Tissier AM, Khairoune A, Khoury G, Eiss D, Helenon O. Ultrasound elastography of the prostate: state of the art. Diagn Interv Imaging 2013;94:551–60.
[29] Woo S, Suh CH, Kim SY, Cho JY, Kim SH. Shear-wave elastography for detection of prostate cancer: a systematic review and diagnostic meta-analysis. AJR Am J Roentgenol 2017;209:806–14.
[30] Anbarasan T, Wei C, Bamber JC, Barr RG, Nabi G. Characterisation of prostate lesions using transrectal shear wave elastography (SWE) ultrasound imaging: a systematic review. Cancers (Basel) 2021;13:122.
[31] Postema AW, Gayet MCW, van Sloun RJG, et al. Contrast-enhanced ultrasound with dispersion analysis for the localization of prostate cancer: correlation with radical prostatectomy specimens. World J Urol 2020;38:2811–8.
[32] Le JD, Tan N, Shkolyar E, et al. Multifocality and prostate cancer detection by multiparametric magnetic resonance imaging: correlation with whole-mount histopathology. Eur Urol 2015;67:569–76.
[33] Johnson DC, Raman SS, Mirak SA, et al. Detection of individual prostate cancer foci via multiparametric magnetic resonance imaging. Eur Urol 2019;75:712–20.
[34] Borofsky S, George AK, Gaur S, et al. What are we missing? False-negative cancers at multiparametric MR imaging of the prostate. Radiology 2018;286:186–95.
[35] Boehm K, Salomon G, Beyer B, et al. Shear wave elastography for localization of prostate cancer lesions and assessment of elasticity thresholds: implications for targeted biopsies and active surveillance protocols. J Urol 2015;193:794–800.
[36] Rouviere O, Melodelima C, Hoang Dinh A, et al. Stiffness of benign and malignant prostate tissue measured by shear-wave elastography: a preliminary study. Eur Radiol 2017;27:1858–66.
[37] Mannaerts CK, Engelbrecht MRW, Postema AW, et al. Detection of clinically significant prostate cancer in biopsy-naive men: direct comparison of systematic biopsy, multiparametric MRI- and contrast-ultrasound-dispersion imaging-targeted biopsy. BJU Int 2020;126:481–93.
[38] Wildeboer RR, Van Sloun RJG, Schalk SG, et al. Convective-dispersion modeling in 3D contrast-ultrasound imaging for the localization of prostate cancer. IEEE Trans Med Imaging 2018;37:2593–602.
[39] Halpern EJ. Contrast-enhanced ultrasound imaging of prostate cancer. Rev Urol 2006;8:S29–37.
[40] Wildeboer R. Blind source separation for clutter and noise suppression in ultrasound imaging: review for different applications. IEEE Trans Med Imaging 2020;67:1497–512.
[41] Lee JJ, Thomas IC, Nolley R, Ferrari M, Brooks JD, Leppert JT. Biologic differences between peripheral and transition zone prostate cancer. Prostate 2015;75:183–90.
[42] Sakai I, Harada K, Kurahashi T, Yamanaka K, Hara I, Miyake H. Analysis of differences in clinicopathological features between prostate cancers located in the transition and peripheral zones. Int J Urol 2006;13:368–72.
[43] Mischi M, Demi L, Smeenge M, et al. Transabdominal contrast-enhanced ultrasound imaging of the prostate. Ultrasound Med Biol 2015;41:1112–8.
[44] Saidov T, Heneweer C, Kuenen M, et al. Fractal dimension of tumor microvasculature by DCE-US: preliminary study in mice. Ultrasound Med Biol 2016;42:2852–63.
[45] Epstein JI, Zelefsky MJ, Sjoberg DD, et al. A contemporary prostate cancer grading system: a validated alternative to the Gleason score. Eur Urol 2016;69:428–35.
[46] Bokor D, Chambers JB, Rees PJ, Mant TG, Luzzani F, Spinazzi A. Clinical safety of SonoVue, a new contrast agent for ultrasound imaging, in healthy volunteers and in patients with chronic obstructive pulmonary disease. Invest Radiol 2001;36:104–9.
[47] Westwood M, Joore M, Grutters J, et al. Contrast-enhanced ultrasound using SonoVue(R) (sulphur hexafluoride microbubbles) compared with contrast-enhanced computed tomography and contrast-enhanced magnetic resonance imaging for the characterisation of focal liver lesions and detection of liver metastases: a systematic review and cost-effectiveness analysis. Health Technol Assess 2013;17:1–243.

[48] Piscaglia F, Bolondi L. Italian Society for Ultrasound in Medicine and Biology (SIUMB) Study Group on Ultrasound Contrast Agents. The safety of Sonovue in abdominal applications: retrospective analysis of 23188 investigations. Ultrasound Med Biol 2006;32:1369–75.
[49] Ozkan TA, Eruyar AT, Cebeci OO, Memik O, Ozcan L, Kuskonmaz I. Interobserver variability in Gleason histological grading of prostate cancer. Scand J Urol 2016;50:420–4.
[50] Melia J, Moseley R, Ball RY, et al. A UK-based investigation of inter- and intra-observer reproducibility of Gleason grading of prostatic biopsies. Histopathology 2006;48:644–54.
[51] Veloso SG, Lima MF, Salles PG, Berenstein CK, Scalon JD, Bambirra EA. Interobserver agreement of Gleason score and modified Gleason score in needle biopsy and in surgical specimen of prostate cancer. Int Braz J Urol 2007;33:639–46; discussion 47–51.